11th European Conference on Earthquake Engineering © 1998 Balkema, Rotterdam, ISBN 90 5410 982 3

Estimation of ground motion by a semi-empirical method using observed records

S. Matsuzaki & S. Kobayashi
Shikoku Electric Power Company, Takamatsu, Japan

Y. Fukushima, M. Mori & T. Watanabe
Ohsaki Research Institute, Tokyo, Japan

Keywords: strong ground motion, active fault, semi-empirical method, observed record, asperity, Median tectonic line, Green's function, response spectrum

ABSTRACT: The semi-empirical approach to the simulation of strong motion using fore- or after-shock records as Green's functions is reliable, however, such records are not available for prediction purposes. Thus we have predicted ground motion for a hypothetical large earthquake from another minor events by adopting a distance correction based on geometrical spreading. Another difficulty in prediction is fault modeling. Surface traces were simplified as fault models 27, 46, 55, and 77 km in length. Further, the actual fault rupturing may be inhomogeneous, so an asperity distribution is assumed. This asperity assumes that dislocation and stress drop are double the average values. No significant difference was seen in the motions estimated by individual models for periods up to 2.0 seconds. This indicates that the dependence of source size is small for strong motion, perhaps as a result of the random summation of high-frequency phases.

1 INTRODUCTION

Since the 1995 Hyogo-ken Nanbu earthquake, the importance of estimating strong ground motion near a fault has been recognized. The methods of carrying out such estimations depend on theoretical, empirical, or semi-empirical approaches. Theoretical methods such as the Haskell model are physically meaningful, but it is very difficult to generate the higher-frequency components above 1.0Hz that have a significant effect on stiff structures. On the other hand, an empirical approach (Kobayashi & Midorikawa 1982) provides estimates of the high-frequency component, but has less physical meaning. A semi-empirical approach using small event record as Green's function (Dan et al. 1990) is a very reliable technique for the high-frequency component, as long as fore or after shock records are obtained. The difficulty with this method for the prediction is obtaining such records. However, rather than fore or after shocks, it is possible to obtain records of small motion. Site and path effects would be included in these records. Further, the source of such small events can be corrected by geometrical spreading. We attempt to simulate strong motion from hypothetical large faults by the semi-empirical method using corrected small records as Green's function.

2 SITE

The site is located on the north shore of the Sada-misaki peninsula, at the western tip of Japan's Shikoku Island. There is a nuclear power plant in the vicinity, so estimation of higher-frequency input ground motion with a frequency above 0.5Hz is very important for safety. The Median tectonic line runs east to west across the island. Lineaments parallel to this line were found in sea front of the site (Tsuyuguchi et al. 1996) by sonic exploration. Some of them are Quaternary active faults. An accerelometer was installed at a depth of 5m in green schist of the Sanbagawa belt. The

site location and near by lineaments are shown in Figure 1. The S-wave velocity of the schist is 2.6km/s by PS well-log interpretation. Although rock near the surface is weathered, it is assumed that the sensor settled on a rock outcrop.

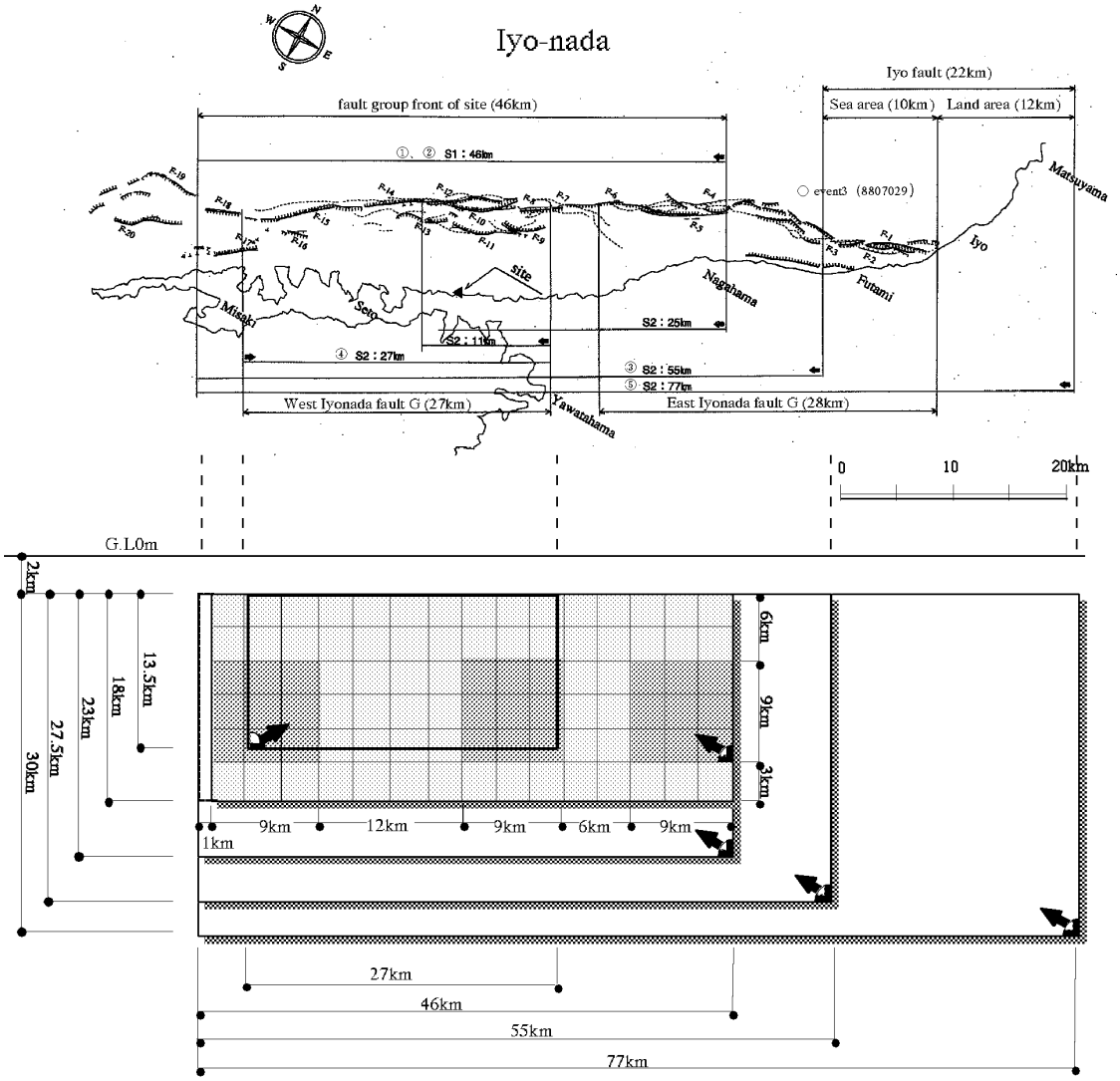

Figure 1. Location of fault traces, site, and epicenter of small event. Section indicates fault models for 27, 46, 55, and 77 km, as well as the asperity model. Arrows indicate rupture initiation points.

3 DATA

As shown in Table 1, records from four events were selected as Green's functions due to their proximity and large peak accelerations. The location of these events, the site, approximate fault, and geology are shown in Figure 2. They did not occur on the fault plane, so the event locations are normalized onto the fault plane by a simple distance correction based on geometrical spreading. Long period noise contaminates the records of events 2 and 4 in period range less than two seconds. Further, event 2 is smaller than M5.0, so it was rejected. On the other hand, event 1 is of large magnitude but was distant from the site, and the ray path of the event crosses three geological belts. For these reasons, records of event 3 are the most suitable to use as the Green's function, and the records are shown in Figure 3.

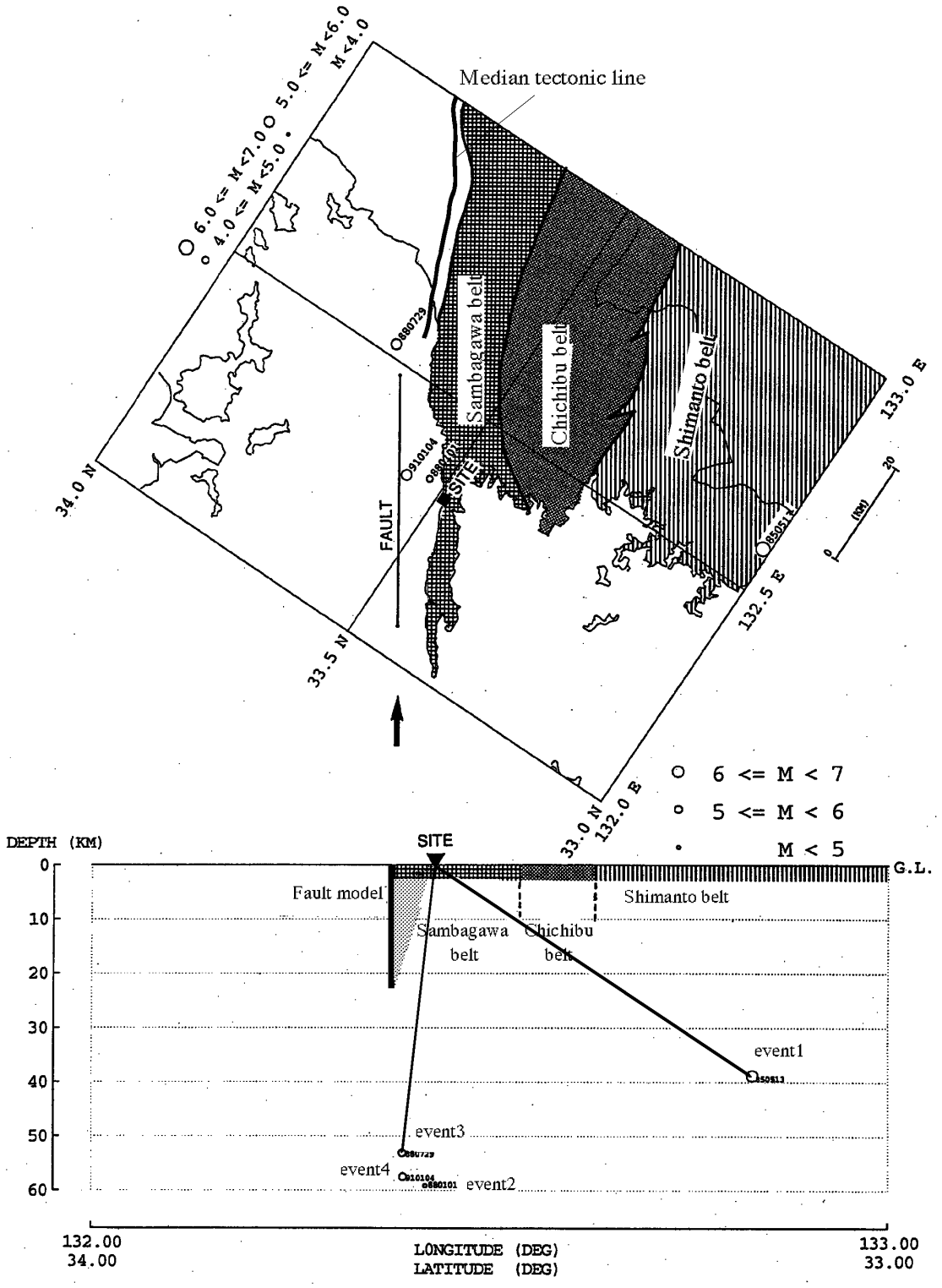

Figure 2. Geology around western Shikoku and event epicenters.

Table 1. Origin of recorded event and peak acceleration.

No.	year/month/day	Lat.	Long.	M	depth.	epicentral distance	PGA
		(N)	(E)		(km)	(km)	(cm/s/s)
1	1985/05/13	32.995	132.587	6.0	39	60	23
2	1988/01/01	33.51	132.34	4.7	59	4	20
3	1988/07/29	33.678	132.508	5.1	53	28	16
4	1991/01/04	33.545	132.322	5.1	58	7	34

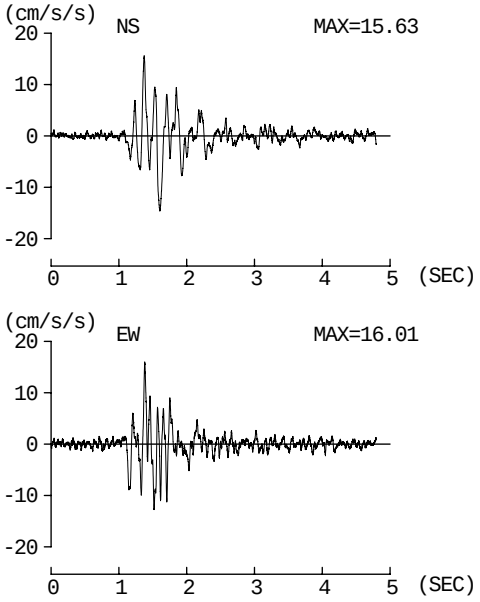

Figure 3. Record of small event 3.

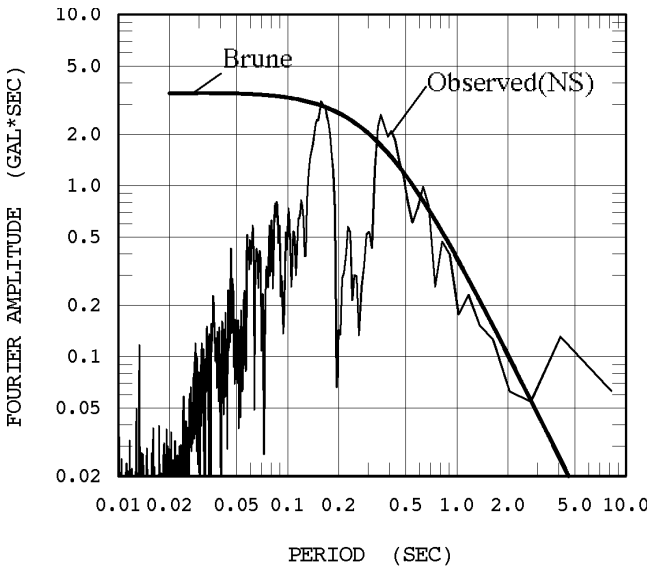

Figure 4. Comparison between Fourier amplitude of observed record and Brune mode.

4 METHOD

As indicated in the introduction, we adapt the semi-empirical method proposed by Dan et al. (1990). First, based on scaling by the ω^{-2} model, dislocation and stress drop of small events are corrected to those of large events in the frequency domain. As a result, longer period component of records than the corner period is according to the large event. The stress drop and seismic moment of the small event were determined by comparison between theoretical (Brune 1970) and observed Fourier amplitudes, as shown in Figure 4. The theoretical amplitude well corresponds with observed amplitude for periods longer than 0.15 second. The derived moment and stress drop of the small event are 5.63×10^{22} dyne*cm and 200 bar, respectively. The ratios of fault length, width, and dislocation between the small and large event are the cube root of the seismic moment ratio:

$$L_L/L_S=W_L/W_S=D_L/D_S=n,\ \ Mo_L/Mo_S=n^3 \qquad (1)$$

Where *L , W, D,* and *Mo* are the length, width, dislocation, and moment, and the suffices *L* and *S* indicate the large and small events. Second, the small events are arranged geometrically on the assumed fault model corresponding to ratio *n*. Then these corrected records are synthesized with arrival time delay to compensate for the rupture propagation process of the large event. The seismic moment derived in the first step was, however, too small to allow deduction of the ghost noise due

to spacial periodicity. Therefore, we synthesize a middle-sized event of 5^3 or 3^3 times the small event assuming a radial rupture. Namely, the moment of the Green's function is increased to 7.04 or 1.52×10^{24} dyne*cm.

5 ASSUMED FAULT MODEL

5.1 *Homogeneous faults*

As shown in Figure 1, we assumed fault models of length of 27, 46, 55, and 77 km, and with widths equal to half the length. The dislocation are assumed to be 210, 363, 420, and 630 cm by an empirical relation (Matsuda 1975). Strike and dip angles are 57 and 90 degrees. The models have an assumed depth of 2 km. Rigidity μ and S-wave velocity are 4.0×10^{11} dyne/cm^2 and 3.5 km/s, respectively. Thus, the seismic moments for the individual models are 0.31, 1.52, 2.54, and 5.82×10^{27}dyne*cm. Taking event 3 as the Green's function, the factor n for the 27, 46, 55, and 77 km models is 4, 6, 7, and 10,respectively. The stress drop is assumed to be 50 bar , which is the average in Japan (Sato 1989). As shown in Figure 1, the rupture initiation points are assumed to be at the deepest point of western end in the case of the 27km model, and otherwise at the eastern ends.

5.2 *Inhomogeneous faults*

Recently, inhomogeneitiy of slip distribution has been revealed in the case of some large events (Wald 1996). Somerville et al. (1993) defined "asperity" areas as elements where the dislocation is two times greater than the average. Our assumed fault size of 46km is almost the same as that in the 1995 Hyogo-ken Nanbu earthquake, and this event exhibited 2 or 3 asperity areas. We also assume a asperity distribution for this 46km model. The width of our model is assumed to be 18km, because the depth of the Conrad discontinuity is 20km around the site. From Somerville et al. (1993), the asperity area is approximately 26% of the total rupture area, so asperity in this case is about 215km^2. Further, Somerville et al. (1993) determined empirical relations between rupture area, seismic moment, and dislocation. From these relations, the moment, average dislocation, and asperity dislocation are estimated to be 2.57×10^{26}dyne*cm, 99cm, and 191cm, respectively. Asperities are likely to occur near segmentation boundary, so we place asperity areas on both sides of the fault model and another at the eastern end of the Iyonada fault group, all with a depth of 6km. The each asperity is 9×9 km^2. The total area of three asperities is almost equal to 26% of the rupture area. The moment for an asperity area is :

$$Mo=\mu LWD=3\times4.0\times10^{11}\ \text{dyne/cm}^2\times81\ \text{km}^2\times191\text{cm}=1.86\times10^{26}\text{dyne*cm} \quad (2)$$

The general scaling is described as equation (1), however the dislocation of asperity D_A is twice as large. Namely:

$$D_A/D_S=2D_L/D_S=2n \quad (3)$$

Therefore, the ratio of small event moment to asperity moment, Mo_A, is

$$Mo_A/Mo_S=2n^3 \quad (4)$$

If we take n=3, the moment of the small event is 1.15×10^{24} dyne*cm, which is little different from the 1.52×10^{24} dyne*cm of the middle-sized event. Namely, the n for dislocation, length, and width of this event is 6, 3 and 3. As shown in Figure 1, the small elements arrange 15 for the length and 6 for the width. The stress drop may be proportional to the dislocation, so 100 bar is assumed for the asperity area. The dislocation for non asperity areas is 30cm because the total moment must evaluate to 2.57×10^{26}dyne*cm. And the stress drop is 15 bar due to the proportionality to the dislocation. The rupture initiation point is the deepest point at the eastern end.

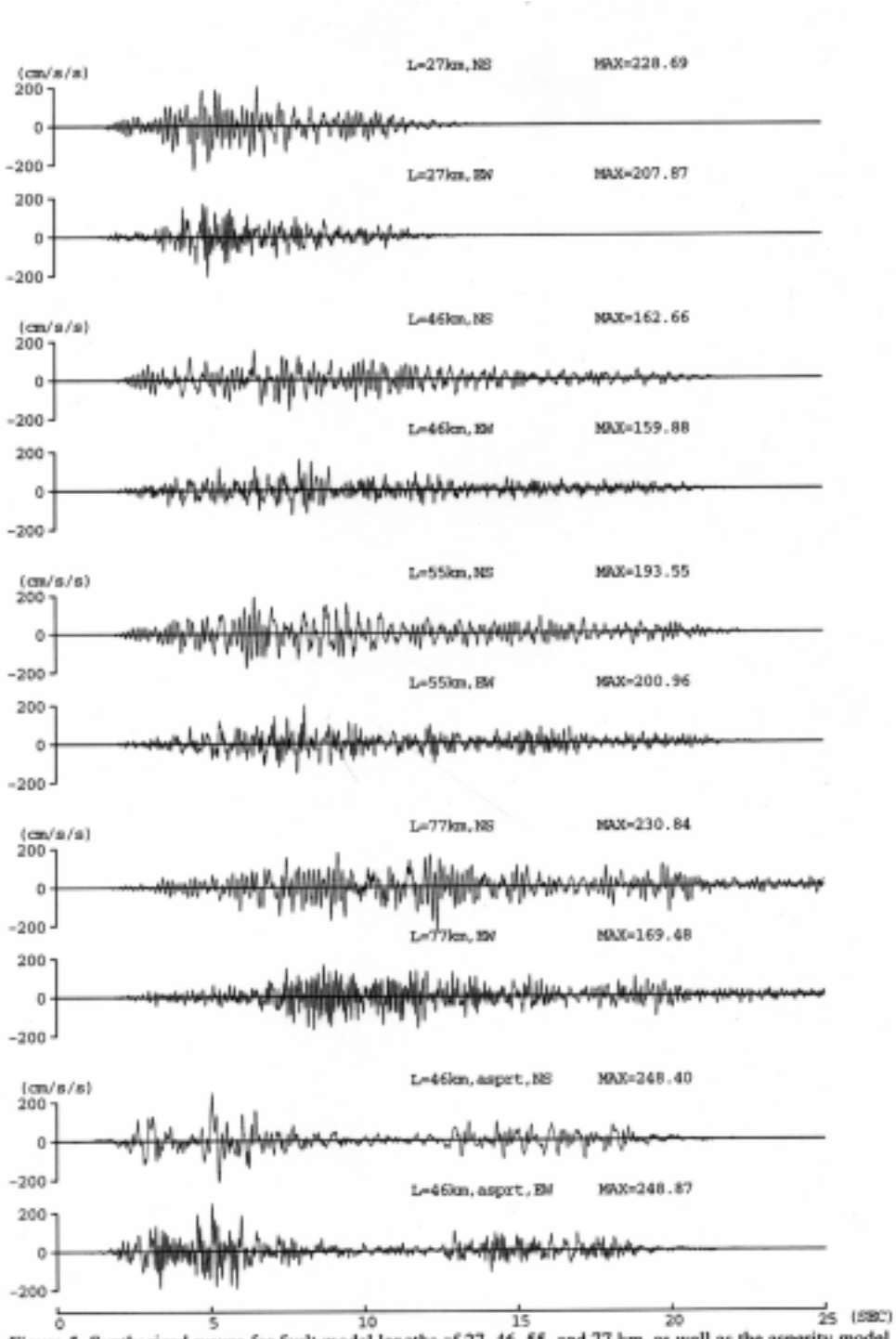

Figure 5. Synthesized waves for fault model lengths of 27, 46, 55, and 77 km, as well as the asperity model

6 RESULTS

6.1 *Waveform*

On the basis of event 3, the synthesized waveforms for the 27, 46, 55, and 77km models, as well as the asperity model, are shown in Figure 5. Duration rises with length of the fault. Three clear phases can be seen in the waveform of the asperity model. The peak amplitude of the asperity model is largest, and about 250 cm/s^2. This may be due to the high stress drop of the asperity. Although, records from the other events are not appropriate as Green's functions, synthesized waves are also derived for the homogeneous model of 46km as a comparison.

6.2 *Response Spectra*

Response spectra of 5% damping for the NS component are shown in Figure 6 for the individual fault length models with a design basis spectrum of the plant. Even as the fault length increases, the responses do not vary much. This indicates that the nearest element effected to the level, independent of source size. The response spectra for the 46 km homogeneous and asperity models are shown in Figure 7. The dips at around 0.3 and 0.8 in the asperity model are shallower than those in the homogeneous model. The response spectra in the case of events 1, 3, and 4 are shown in Figure 8. The dispersion is large, but each spectrum is smaller than the design spectrum.

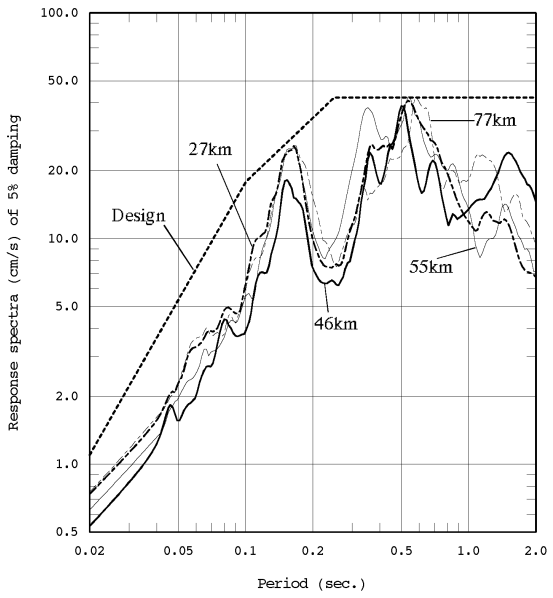

Figure 6. Response spectra of 5% damping of NS component for fault model lengths of 27, 46, 55, and 77 km, as well as design spectrum.

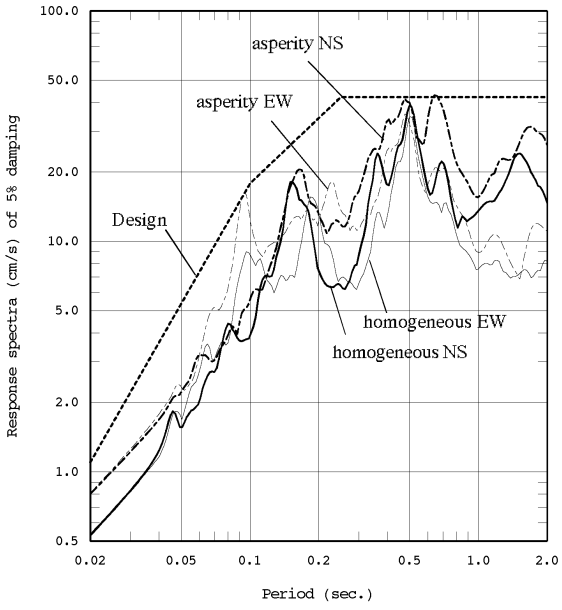

Figure 7. Response spectra of 5% damping for 46 km homogeneous and asperity models, and design spectra.

7 CONCLUSION

Response spectra for all the synthesized waveforms are smaller than the design spectra, and there are no significant differences in the estimated ground motions for the individual fault lengths. This indicates that the effect of source size is relatively small for strong ground motion of short period due to the random summation of the high-frequency phase. For the same reason, directivity may less affect the high frequency component. Only the dips in the spectrum for the asperity model are

shallower than those of the homogeneous model. This may be due to inhomogeneity and the inclusion of various frequency components in the synthesized waveform.

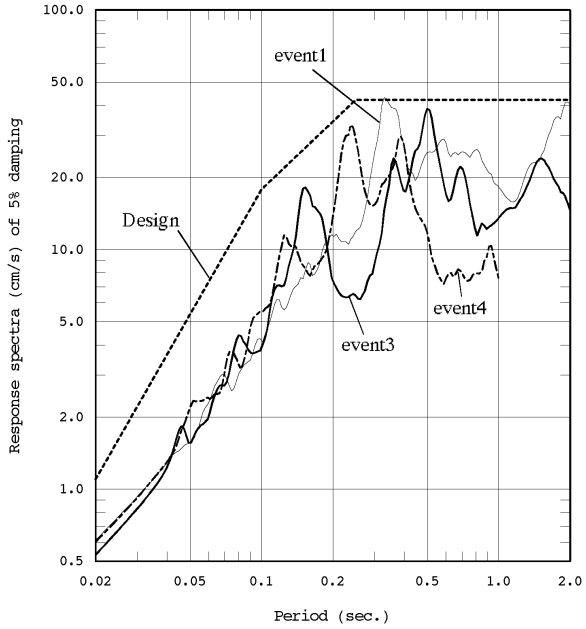

Figure 8. Response spectra of 5% damping for model length of 46 km, and design spectrum. Green's functions are NS component of events 1, 3 and 4.

ACKNOWLEDGMENT

We acknowledge with gratitude the valuable help provided by Prof. K. Irikura of the Disaster Prevention Research Institute, Kyoto University.

REFERENCES

Brune, J. 1970. Tectonic stress and the spectra of seismic shear waves from earthquakes, *J. Geophys. Res*., 75, 4997-5009.

Dan, K. et al. 1990. Stability of earthquake ground motion synthesized by using different small-event records as empirical Green's functions, *Bull. Seism. Soc. Am.*, 80, 1433-1455.

Kobayashi, H. & S. Midorikawa. 1982. A semi-empirical method for estimating response spectra of near-field ground motions with regard to fault rupture, *Proc. 7th European Conf. on Earthq. Eng.*, 161-168.

Matsuda, T. 1975. Magnitude and recurrence interval of earthquake from a fault, *Zishin* 2, 28, 269-283.(in Japanese)

Sato, R. 1989. Fault parameter handbook in Japan, Kajima-shuppankai, Tokyo. (in Japanese)

Somerville P. G. et al. 1993. A study of slip distribution in earthquuake fault, *Proc. 23 JSCE Earthq. Eng. Sympo., Japan Soc. Civil Eng.*, 291-294. (in Japanese)

Tsuyuguchi, K. et al. 1996. Distribution and segmentation of submarine active faults of Median Tectonic Line, Iyonada, *Abstracts the 103rd Annual Meeting of the Geol.Soc.Japan*, p364. (in Japanese)

Wald, D. J. 1996. Slip history of the 1995 Kobe, Japan, earthquake determined from strong motion, teleseismic, and geodetic data, *J. Phys. Earth*, 44, 489-503.